THE UNIVERSITY OF WARWICK

"Detection of cracks in metal sheets using pulsed laser generated ultrasound and EMAT detection"

S. Dixon, S.E. Burrows, B. Dutton and Y. Fan

Department of Physics, University of Warwick, Coventry, CV4 7AL, UK.

Abstract

A pulsed Nd:YAG laser with an approximately Gaussian beam shape is directed onto the surface of an aluminium sheet at an energy density below which damage by laser ablation occurs, generating Lamb waves in the sheet. The laser beam is raster scanned across the surface of the sample. The Lamb waves travel radially outwards from the generation point and are detected some distance away by an electromagnetic acoustic transducer with sensitivity to in-plane displacements of the sheet. A number of static EMATs are located around the edges of the sheet, some distance from the generation point. The presence of a crack-like defect on the sheet can be detected by either a sudden change in the ultrasonic waveform or by an enhancement in the frequency content of the waveform when the laser beam illuminates directly onto the crack.

Keywords : laser ultrasound, lamb waves, EMATs

1. Introduction

Laser generated ultrasound [1-8] has for some time been used in research laboratories as it provides a non-contact, wideband and controllable generation source capable of simultaneously generating compression, shear and surface waves on a range of materials. A number of different types of pulsed lasers can be used to generate ultrasound [4], but the most common is probably the solid-state pulsed Nd:YAG laser, for many applications.

At high energy densities, typically greater than 10^6 Wcm^{-2} on metals, a pulsed laser beam will ablate the surface of the sample [4], removing material down to a depth of several microns over the irradiated area. In some applications this level of damage is tolerable, but in general it is desirable to have a completely non-destructive ultrasonic generation mechanism. This is achieved by reducing the energy density of the pulsed laser below the threshold of ablation, and such a source is described as thermoelastic.

The laser pulse typically is between 5 ns to 100 ns long, although much faster pulses have been used to generate ultrasound [9]. The frequency content of the waves generated by the pulsed laser beam is dependent on a convolution of the spatial and temporal properties of the source. Laser pulses of 10 ns duration are capable of generating broadband ultrasonic waves with measurable frequency content up to 100MHz, although wave attenuation and the width of the source mean that measured waves will usually have lower frequency content. In this work a frequency doubled Nd:YAG laser with a wavelength of 532 nm, a pulse width of 10 ns, an energy of 800 mJ and a beam diameter of approximately 6 mm is used to generate the Lamb waves in the metal sheet.

In the thermoelastic regime, the area of the sample illuminated by the laser beam is heated rapidly by the absorption of the laser energy. The heated region expands and generates stress as the surrounding cooler material constrains the expansion of the heated region. The exact distribution of this force is dependent upon the energy density profile of the incident laser beam, but the resultant force is predominantly in-plane as the surface of the heated region is free to expand into the air region above it [3,4]. The laser beam energy is absorbed within the electromagnetic skin depth, which for light of 532 nm is approximately 4 nm in aluminium. Because metals have a relatively high thermal conductivity, the effective depth of the heated region of the source will extend slightly beyond the electromagnetic skindepth [4]. The effective depth of the source is many orders of magnitude smaller than the highest frequency ultrasonic waves that are detectable, with the result that one can treat the laser generated ultrasonic source as purely a surface force.

The principle that the laser based source on metals is purely a surface acting source has certain implications for the properties of the Lamb waves that will be generated. Certain Lamb wave modes at particular frequencies have relatively small or even zero in-plane displacement at the surface. Such

modes will not be efficiently generated by a pulsed laser beam source. In what follows, we assume that the sample is an isotropic plate or sheet and that the reader is familiar with the fact that a metal sheet will support guided Lamb wave modes that can be split up into two distinct types; symmetric and anti-symmetric modes. Any force acting on a one side of a plate or sheet is capable of generating both symmetric and anti-symmetric Lamb wave modes. The explanation for this is that one can represent any force, F, acting on one side of a plate, into the sum of a purely symmetric force and a purely anti-symmetric force acting on each side of the plate [10], each of magnitude, F/2. The schematic diagram of figure 1 explains why this is the case.
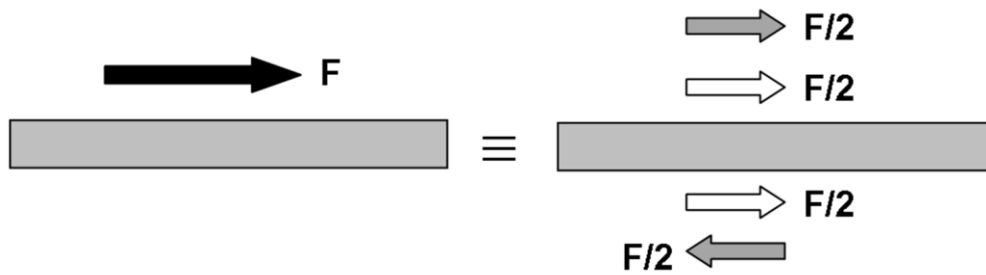
Figure 1

The force acting on surface of the sample on the left (black arrow) is equivalent to the sum of the purely symmetric (white arrows) and purely anti-symmetric (grey arrows) acting at the same point on the surfaces of the sample on the right.

The purely anti-symmetric force will generate only anti-symmetric mode Lamb waves, and the purely symmetric force will generate only symmetric mode Lamb waves. In determining how efficiently the in-plane force at the surface generates a particular mode at a particular frequency, one needs to consider the relative displacement amplitude of that particular mode. For example, the relative magnitudes of the in-plane and out-of-plane displacements are shown in figure 2 for the symmetric zero order S_0 mode Lamb wave at frequency-thickness products of 0.5 MHz-mm and 2.21 MHz-mm; these are for nominally pure aluminium sheet with compression and shear wave velocities of 6320 ms^{-1} and 3130 ms^{-1} respectively. From figure 2, one can see that that the S_0 mode should be generated more efficiently by the laser source at the frequency thickness product of 0.5 MHz-mm when compared to

2.21 MHz-mm, where there is almost zero in-plane displacement at the surface. These have been

calculated using the standard technique of firstly solving the relevant Rayleigh-Lamb equations to find

the phase velocity of a particular mode at a particular frequency thickness product, and then taking this

result to calculate the displacement through the thickness of the plate [11].
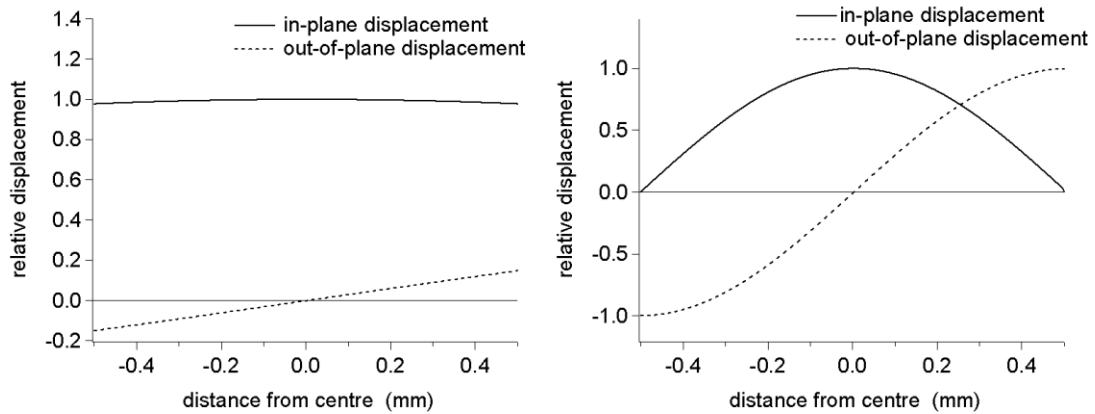

Figure 2

Relative displacement of the in-plane and out of plane components in a 1 mm thick aluminium sheet

for the S_0 mode Lamb wave at frequency-thickness products of 0.5 MHz-mm (left) and 2.21 MHz-mm

(right).

Electromagnetic acoustic transducers (EMATs) are capable of either generating or detecting ultrasonic

waves at the surface of a sample that is either electrically conductive or has favourable magnetic

properties. Favourable magnetic properties typically means that the sample will have a high

magnetostrictive coefficient [12,13]. The EMAT is coupled to the sample by electromagnetic waves

and thus their operation is non-contact, and they are generally wide bandwidth devices, capable of

detecting signals of frequencies greater than 100MHz.   Here, the EMATs are used to detect ultrasonic

Lamb waves that have propagated from the generation point to the detection point, on an aluminium

plate. EMATs are velocity sensors [14,15] and as they are non-contact, they do not significantly

mechanically load the sample that is being measured, so that their influence on the properties being

measured is negligible. EMATs need to be within several millimetres of the sample surface as the

detection efficiency falls off dramatically with increased stand-off of the transducer from the sample.

There are several previous examples in the published literature [16-20] of researchers using a pulsed laser to generate ultrasound which is subsequently detected using an EMAT. The EMAT has favourable sensitivity when compared to laser based interferometric detection [21], particularly where in-plane displacement measurements are measured.

2. Experimental Method

The experimental set-up is shown below in the schematic diagram of figure 3. The sheet metal sample is held stationary and a number of EMATs are placed in close proximity to the sample surface such that the transducers almost touch the sample surface. The laser beam is incident on a computer controlled, two axis gimballed mirror that scans the pulsed laser beam impact point across the sample surface. In some samples, a small slot has been laser machined into the sample at an angle normal to the surface of the sample.
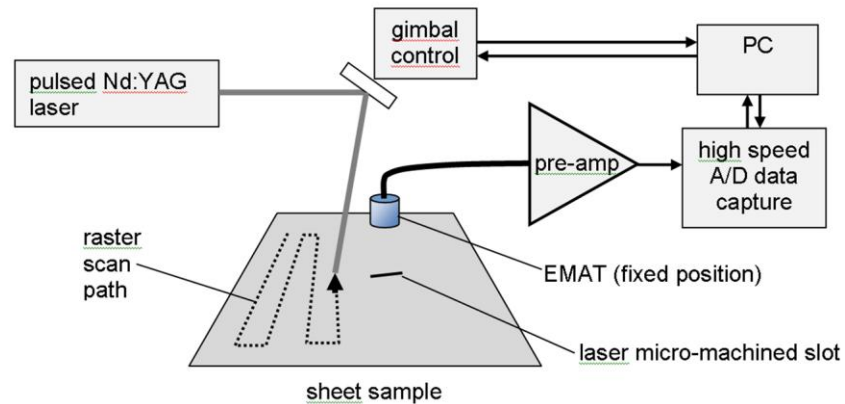

Figure 3

Schematic diagram of experimental set-up used for non-contact detection of cracks in sheet metal plate.

When the simulated defect lies between the generation point and the detection point, there will clearly be a strong effect on the detected signal. One might reasonably expect that this effect is largest when the generation point is very close to the defect as this will minimise the amount of energy that can diffract around the defect. The effect of passing the source over the defect is examined by scanning the laser beam along a line towards the EMAT starting with the defect between the generation and detection point.

The EMAT is a linear coil, constructed by wrapping a single layer of 0.08 mm diameter insulated copper wire around a 35 mm diameter NdFeB, cylindrical permanent magnet. The total width of the coil is 2 mm and the length of the coil is equal to the diameter of the cylindrical magnet. A schematic diagram of the EMAT construction in shown in figure 4. The cylindrical magnet and surrounding coil are held in a brass case and the front of the EMAT coil is protected by a 0.5 mm thick polymer sheet.
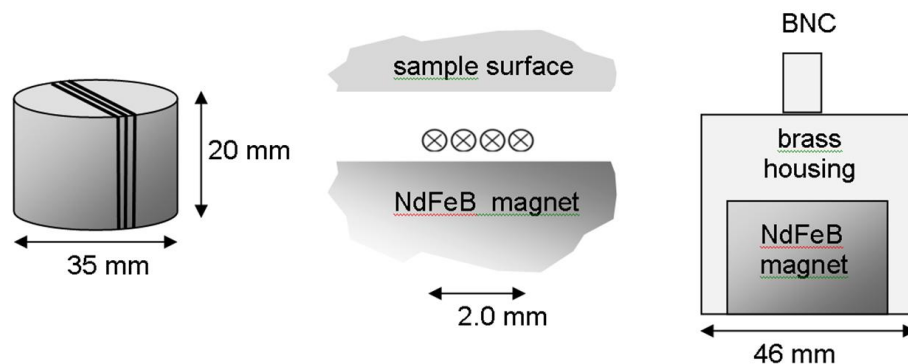

Figure 4

Schematic diagram of EMAT construction. Note that the various features shown are not to scale and the number of turns of the coil is fifteen.

The EMAT is connected to a wideband pre-amplifier with a gain of approximately 60dB for frequencies between 0.1 MHz – 5 MHz. The pre-amplifier is connected to either a digital oscilloscope or a PC based data acquisition card. In each case, the analogue bandwidth is 100 MHz, and the digitisation rate is 100 Msamples per second at 8-bits resolution. The data is stored on a computer for signal processing. Note that the 2 mm width of the EMAT coil limits the bandwidth of the sensor, due to the spatial impulse response effect [22]. The EMAT will not detect significant or representative

signal amplitudes for signals of less than 2 mm wavelength, and for wavelengths around this value there will be resonant effects on the detected signal.

Aluminium sheets of between 0.5 mm to 3 mm thick are used to study the behaviour of the laser generated Lamb waves as they propagate along a defect free plate. A 10 mm thick 304 stainless steel plate is also examined, containing a simulated stress-corrosion crack of estimated size 3+/- 0.6mm deep with an average gape of 24μm wide. The size of the defect was established from destructive tests of control samples and verified by alternating current potential drop (ACPD) measurements [23].

The experiments are also modelled using a finite element software package, PZFlex, for the case where the defect lies roughly midway between the generation and detection points which are separated by 8.5cm. This was performed for comparison with experimental observations and to illustrate that the wideband Lamb wave can readily diffract around a defect.

3. Results

There are a number of factors that one should consider when analysing ultrasonic waveforms detected by EMATs. This particular EMAT is sensitive to in-plane ultrasonic displacements and because it is a velocity sensor, the detected signal will have larger magnitudes at higher frequencies when compared to the true displacement waveform [14, 15, 24]. A single frequency component of the displacement, A, of a one dimensional wave can be written

$$A \; = \; A_0 \, e^{i(\omega t - kx)} \qquad\qquad 1$$

where ω is angular frequency, k is wavenumber, t is time and x is distance. Thus the velocity of a particle as the wave passes is obtained from differentiation of the term above giving

$$\frac{dA}{dt} \; = \; \dot{A} \; = \; -i\omega A_0 \, e^{i(\omega t - kx)} \qquad\qquad 2$$

Thus, the EMAT detected signal is enhanced by a linear factor of frequency when compared to the true displacement. If the ultrasonic amplitude is required from the EMAT detected signal, a pre-amplifier with constant gain over the bandwidth of the signal must be used before the data is processed.

The EMAT coil has a small but finite width, 2 mm in this case. The finite width of the coil will make the detected signal appear differently to the signal that would be detected by an infinitely narrow coil.

When the width of the sensor becomes comparable to the wavelength of the wave passing underneath the coil, the signal detected by the EMAT will not be a true representation of the velocity of the particles in the sample associated with the propagation of the wave. This effect is sometimes referred to as the spatial impulse response, and can be crudely modelled by considering what happens when a sine wave passes under a finite width coil.

For a single frequency wave, the velocity of the particles in the surface can be written as in equation 2 above. For a coil with uniform sensitivity across a coil of width L, located close to the surface of the sample, one can write the total voltage signal induced in the coil, V_c, as the integral of equation 2 across the coil such that

$$V_c \quad \propto \quad \int_{x=-L/2}^{x=+L/2} e^{i(\omega t - kx)} \, dx \qquad\qquad 3$$

or

$$V_c \quad \propto \quad \frac{e^{i(\omega t)}}{k} \quad \sin\left(\frac{kL}{2}\right) \qquad\qquad 4$$

One can consider either the time average or maximum value of this function. Considering the maximum value, V_{cmax} this function takes on with varying time one can write

$$V_{c\max} \quad \propto \quad \frac{1}{k} \quad \sin\left(\frac{kL}{2}\right) \qquad\qquad 5$$

Plotting the modulus of the function described by equation 5 for a coil width of 2mm yields figure 5; this shows the normalized maximum amplitude response for a sinusoidally varying wave as the wavelength is varied.

In plotting figure 5, any amplitude enhancement due to the EMAT being a velocity sensor has been ignored as for Lamb waves there is a range of modes that can exist; within this range, modes of the same wavelength can have different frequencies, and phase and group velocities are very different in general. The purpose of this plot is mainly to demonstrate that sensitivity of the EMAT will in general reduce as wavelength shortens if all other factors remain the same. For wavelengths below one half of the coil width, the response falls to below 10% of the long wavelength limit.
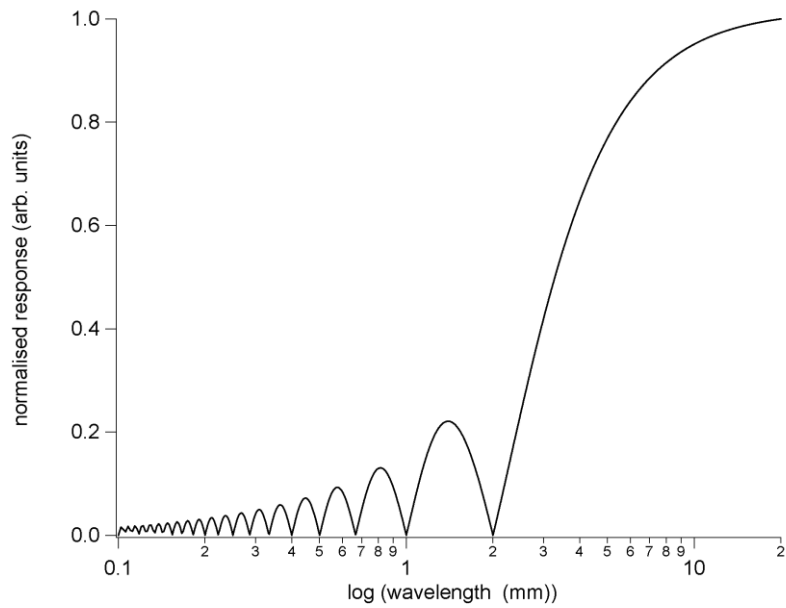
Figure 5

The modulus of the response is plotted as a function of frequency, normalised to the long wavelength limit of 1. Note that the first minima occurs when the coil width is equal to the wavelength as expected and that the response drops to 50% of its maximum value when the wavelength is 50% larger than the coil width.

3.1.1 Experimental results on defect free aluminium sheets

Laser generated Lamb waves are generated and detected on a range of nominally pure, defect free aluminium sheets of different thickness in the range of 0.5 mm to 7 mm thick, using the laser-EMAT system. The EMAT detected signals are shown in figure 6a –g, where the distance between the EMAT and laser beam is approximately 8.5 cm in each case. In some of the thicker plates it is clear that features of a very similar frequency run throughout the waveform and these can be associated with particular Lamb wave modes. There are approaches that can attempt to time-reverse these types of signals [25] assuming particular dispersion properties of the plate, but in this case we are interested particularly in using these signals to identify the presence of a defect and if possible characterise the defect.
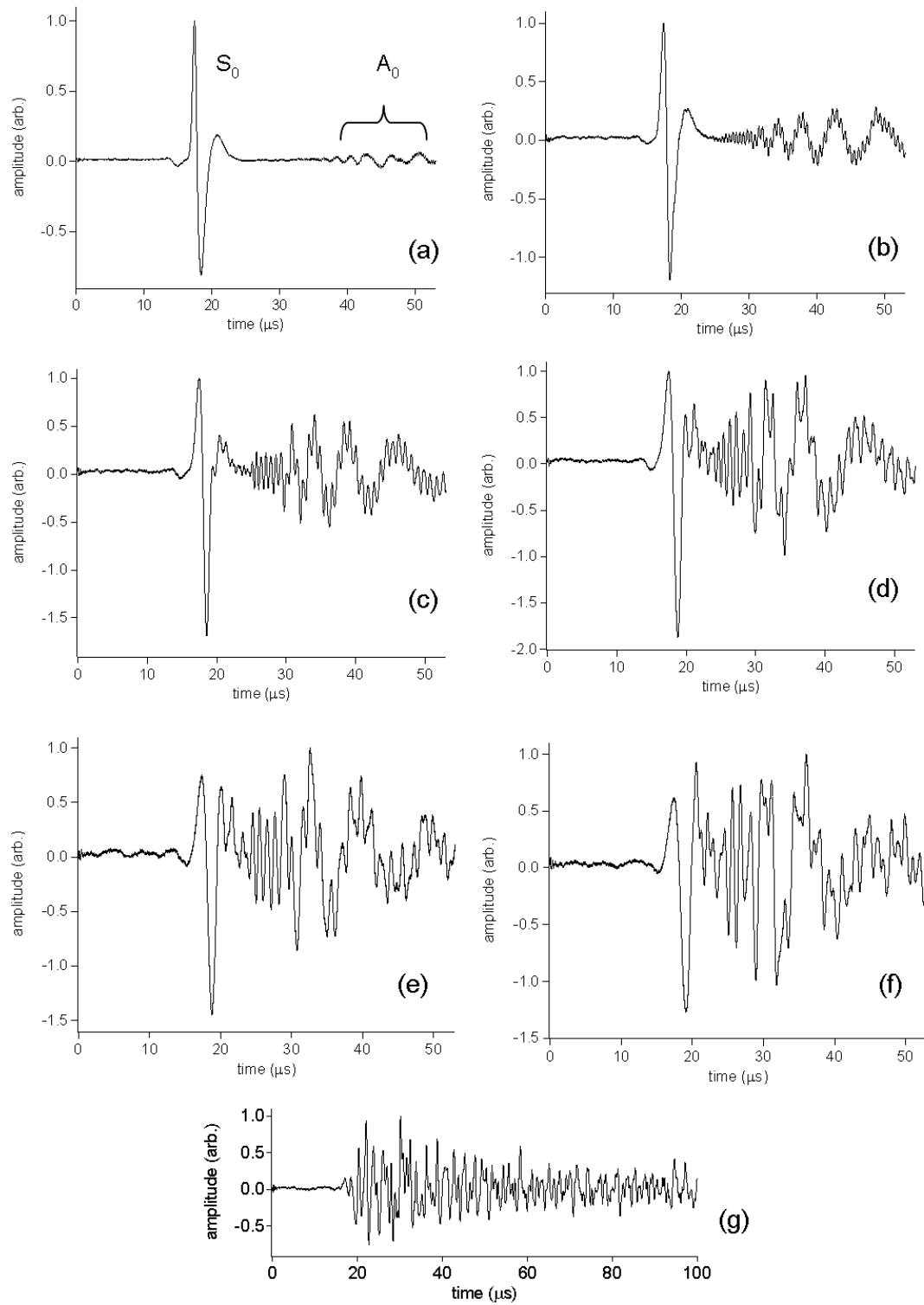
Figure 6

A-scan waveforms of laser generated ultrasound on aluminium sheets of different thickness. (a) 0.5mm (b) 1.0mm   (c) 1.5mm (d) 2.0mm (e) 2.5mm (f) 3.0mm (g) 7.0mm. Note that amplitude refers to the amplitude of the signal from the pre-amplifier and is not the amplitude of the ultrasonic displacement.

The 0.5 mm thick sheet clearly shows the S_0 and the A_0 modes. In the long wavelength limit [16,17], these are the only two modes that can be observed, but as the laser generated ultrasound is very wideband, with a rise-time of 10 ns, a higher a higher order mode can be observed on the waveform of figure 6a, running through the A_0 mode as a higher frequency oscillation. Even though the pulsed laser is a very wideband source, capable of generating wave-modes with frequencies in excess of 100 MHz, the spatial extent of the generation source and especially the spatial extent of the EMAT detection coil, limit the minimum wavelength of wave that can be detected. As expected, thicker plates support a larger number of modes that can be detected using the EMAT, and so the waveforms appear progressively more complex as plate thickness increases. The waveform that is recorded on the 7mm thick aluminium plate is shown in figure 6g, to illustrate this point and is shown over a longer timescale. Investigating different methods of interpreting multimode Lamb wave signals has generated many different research publications, including methods using wavelet analysis [26-28].

The magnitude Fast Fourier Transforms (FFTs) for these waveforms of figure 6a-f are shown in figures 7a-f. These FFTs show some common characteristics, notably the apparent appearance and decay of peaks over particular frequency ranges. The first peak is associated with the S_0 and the A_0 modes. Subsequent peaks are associated with the appearance of higher order modes.

The first FFT of figure 7a shows a distinct peak at approximately 0.5 MHz and a small second peak at approximately 3.3 MHz. As sheet thickness increases, it appears that these peaks shift to lower frequencies, the spacing between the peaks decreases, and more peaks appear in the FFT. The structure of each peak is itself complicated, particularly the first and largest peak occurring at the lowest frequency, which contains many minor peaks or oscillations. These sources of these various features are explained in more detail in the following.

The group velocity for the symmetric and anti-symmetric modes has been calculated by the standard approach of solving numerically the Rayleigh-Lamb equation [11] for isotropic sheets. The group velocity plots for the modes for the 1 mm and 3 mm thick sheets with the corresponding FFTs of figure 7 directly below them are shown in figure 8. Note that the horizontal axes have been changed to MHz-mm to allow comparison.
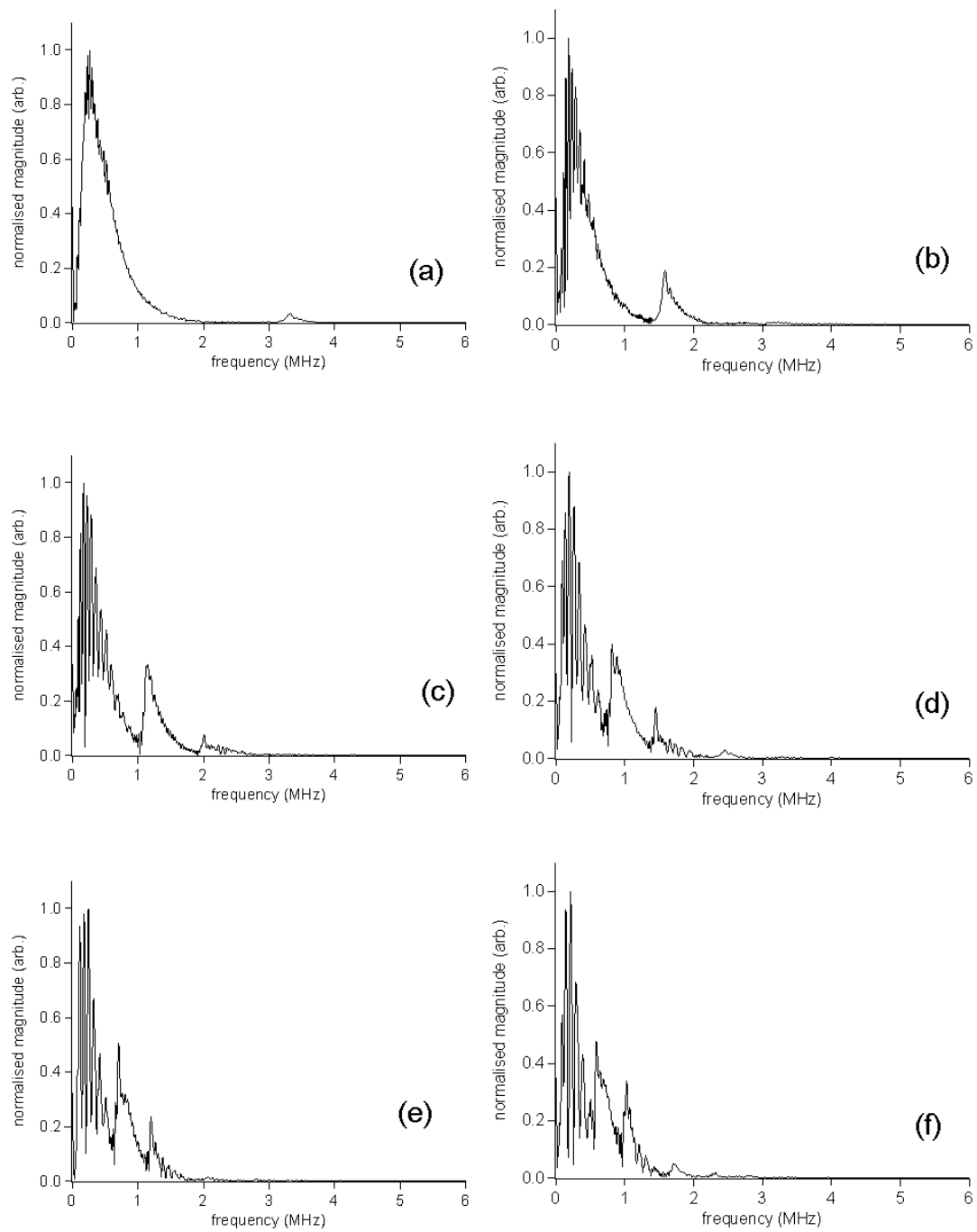
Figure 7

The magnitude FFTs for the A-scan waveforms shown in figure 6. There are a distinctive number of peaks within each FFT, that correspond to different Lamb wave modes.
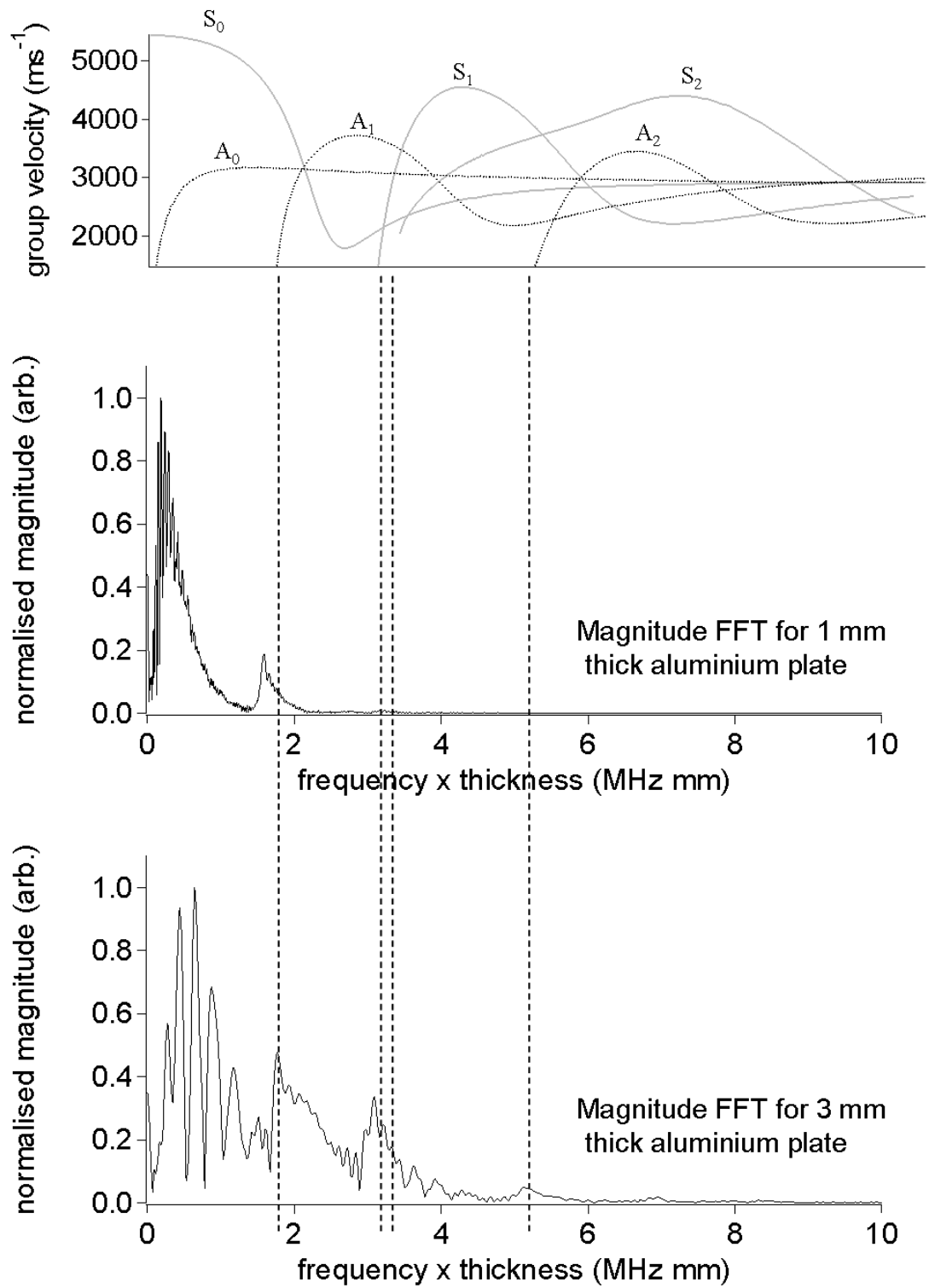
Figure 8

Magnitude FFT of 1 mm and 3mm sheets together with the Lamb wave group velocity dispersion curves. Note that in this case the horizontal axes are in MHz-mm.

The very first peak in the FFTs of figures 7 and 8 cannot have significant frequency content at very low frequencies, partly because the size of the window in which the data is initially captured is 100 μs, but more importantly because the preamplifier used to amplify the EMAT signals has a low frequency cut off for frequencies below 50 kHz. The temporal size of the window also determines which modes can be observed, because certain modes or parts of modes with lower group velocities will fall outside the data capture window. In this case only data below 50 μs is Fourier transformed, and with a laser beam – EMAT separation of approximately 8.5 cm, this corresponds to a velocity of approximately 1600 ms^{-1}. Thus, one should only consider modes with group velocities above this value and this is why the group velocity plot of figure 8 is cropped on the velocity axis.

The complex structure of the first peak in the FFT arises because this peak consists of contributions from both the S_0 and the A_0 modes, and these interfere in the frequency domain. This effect is described in more detail in the discussion of figure 9. Other peaks will also show more complex structure because they too can consist of contributions from different modes. A further point to note for the peaks in the FFTs is that in each main peak observed in the FFTs of figure 7 and 8, the low frequency edge of the peak is relatively steep and this is then followed by a more gradual decay. The relatively steep leading edge arises because beyond a certain threshold, a higher order mode can exist. This gradual decay arises because at higher frequency-thickness products for a particular mode, there is a tendency for the wavelength of the mode to decrease, and as discussed earlier and as shown in figure 5, the EMAT sensitivity decreases due to the spatial impulse response effect.

It is clear that the second peak in figures 8 at approximately 1.75 MHz-mm, corresponds to the appearance of the A_1 mode. Closer examination of the waveforms of figure 6 for the 0.5 mm and 1.0 mm thick sheets, shows that there is an oscillating signal of an almost constant frequency running throughout the region after the arrival of the S_0 mode. This is because the group velocity curve for this mode is very steep in this region, meaning that there is a large range of velocities for this mode over a relatively small frequency range, below a frequency – thickness product of 2 MHz-mm. The third peak or double peak in figures 8, at a frequency – thickness product of approximately 3.25 MHz-mm, corresponds to the appearance of the S_1 and the S_2 modes. The fourth peak, which is visible in the magnitude FFT for the 3 mm thick plate, at a frequency – thickness product of approximately 5.25 MHz-mm, corresponds to the appearance of the A_2 mode.

We are thus able to explain and understand the appearance of the magnitude FFT of the waveform, although this becomes more complex as plate thickness increases. The reader should note that the authors do not advocate this method as a general approach for the signal processing of Lamb wave modes. The magnitude FFT does have some disadvantages in that on its own; it does not show where the magnitude associated with a particular frequency lies within the time domain waveform. One could consider Short Time Fourier Transforms STFT [28] or wavelet analysis [27] for this type of operation, but each of these has its own drawbacks, most principally being that some a-priori knowledge of the properties of the signal being detected is really required. The potential for using the FFT to analyse the data for crack detection is considered, because the FFT is a relatively simple mathematical operation and is easily implemented into both software and hardware signal processing approaches. The FFT also demonstrates that there is some enhancement of higher frequency components of the Lamb waves when the pulsed laser beam impinges on a crack as will be discussed later.

The FFTs of figure 7 all show a characteristic behaviour in that there is a low frequency asymmetric peak extending out to approximately 1.75 MHz. This peak has some structure that is due to the periodicity of frequency components from the different modes. This can be demonstrated by applying an FFT to the waveform obtained on the 1mm sheet, where the S_0 mode alone, the A_0 and then the entire A-scan are windowed and FFT'd. The result of figure 9 shows that the magnitude FFT of the windowed S_0 mode is relatively smooth, and that of the windowed A_0 and A_1 modes is also relatively smooth compared to the magnitude FFT of the entire waveform. The magnitude FFT of the entire waveform containing both the S_0 and the A_0 modes has a peak that is of similar overall shape to that of the S_0 modes, but it also contains oscillations, that in this case correspond to the periodicity between frequency components in the S_0, A_0 and the A_1 modes.

Some readers will be very familiar with this effect, but it was thought worth mentioning here to ensure that the structures of the peaks in the FFT are understood. The first and largest peak in the FFT is followed by a number of small asymmetric peaks, the number and position in the frequency domain of which is dependent on the sheet thickness.
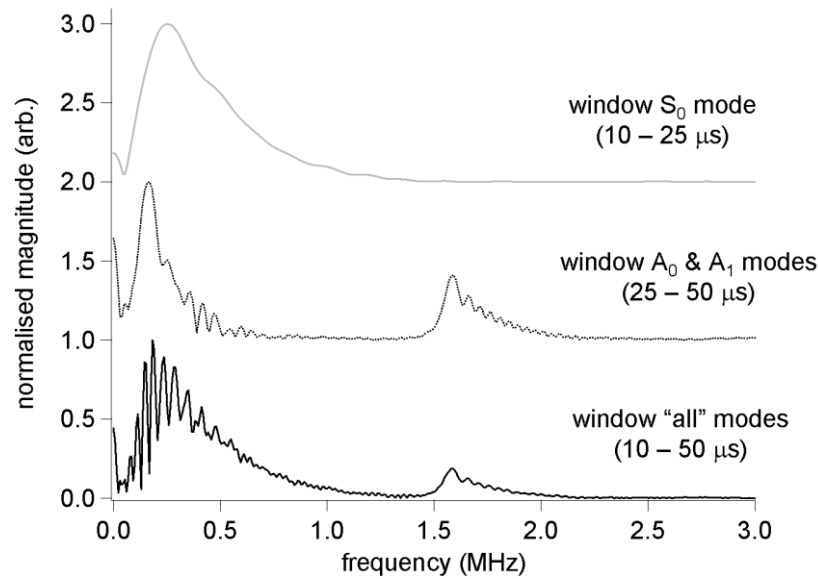
Figure 9

FFT of various parts of the waveform obtained on 1 mm thick aluminium sheet of figure 6b. Note that the purest mode windowed is that, shown in the topmost FFT.

3.1.2 Experimental results on defective aluminium sheets

An Oxford Lasers E-355H laser micro-machining system was used to manufacture a very narrow slot in a 2mm thick aluminium plate. The slot extended down to a depth of 1.2mm with a length of 25mm and gape of 40μm.

The simulated defect is orientated parallel to the direction of the EMAT coil and perpendicular to a line along which the laser beam is scanned and which bisects the defect as shown schematically in the plan view of figure 10.

In order to visualise changes in the detected signal as the laser beam is scanned over the sample and the defect, the data is presented in the form of a B-scan. At each laser beam position, the detected time domain waveform, or A-scan, is measured and stored. These A-scans are then coded such that the amplitude is assigned a corresponding greyscale value. These strips are then stacked side by side to form a B-scan. B-scans are also formed by stacking together a number of magnitude Fourier transforms, again whose amplitudes are assigned a greyscale value.
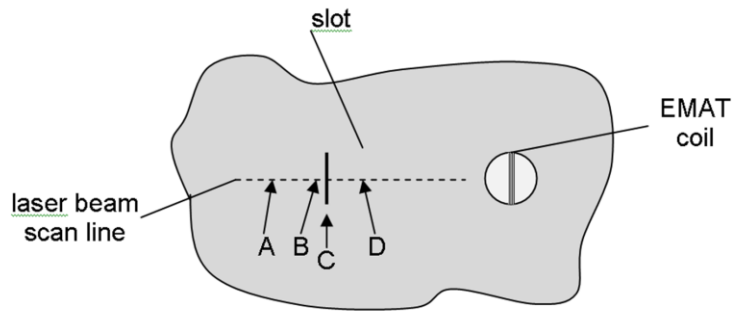
Figure 10

Schematic diagram of plan view of a line scan experiment on a plate containing a simulated defect of length 25mm.

The B-scans of the time and frequency domain data from two 2mm thick sheets, one of which contains a laser micro-machined slot, are shown in figure 11 a-d.

The alignment of the laser and EMAT is slightly different between the scans taken on the defect free sheet and the sheet containing the slot. This gives rise to some of the differences observed in the B-scans of figures 11a and 11b, most notably the different gradients of the linear features within the images, which are not of importance for the following discussion. Locations B and C as shown in figure 10 are approximately positioned at the arbitrary locations 10-12 in the B-scans of figure 11. The B-scans of figures 11c and 11d clearly show the oscillations that were shown in figure 9 and explained in the discussion of figure 9.

It should be noted that there is a clear disruption in the time and frequency domain B-scans around the location of the slot. Equally importantly, there are clearly significant levels of measured signal when the slot lies between the laser beam and the EMAT, indicating that there is significant diffraction of the Lamb waves both around and under the slot. Thus one can only rely on detecting the presence of the defect when the laser beam is very close to, or over the slot.

This result is partly intuitive as one might reasonably expect the laser generated Lamb waves to be blocked most effectively from travelling to the detector when the source is very close to the slot, and the slot is between the laser beam and the EMAT detector. What is perhaps more surprising is the clear frequency enhancement of higher frequencies when the laser beam impinges upon the slot. This is seen as a significant increase in amplitude of the higher frequency components of figure 11c around

locations 12 and 13. Similar behaviour, in terms of an increase in the magnitude of higher frequency components has been reported previously when performing similar experiments on thicker samples where Rayleigh waves are generated [29-31].
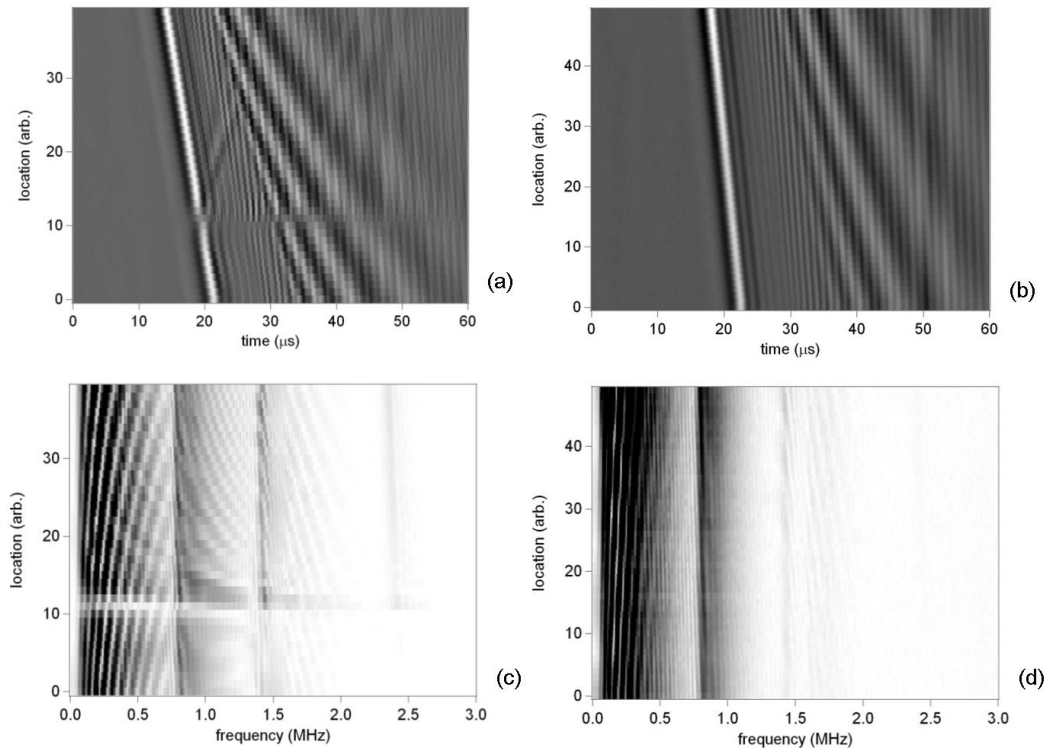

Figure 11

The B-scan of the time domain (A-scan) waveforms for the sheet containing the slot and the defect free sheet are shown above as (a) and (b) respectively. The B-scan of the frequency domain (magnitude FFT) waveforms for the sheet containing the slot and the defect free sheet are shown above as (c) and (d) respectively.

Some of the A-scan waveforms from the plot of figure 11a, together with their respective FFTs are shown in figure 12. The labels A-D correspond to the approximate positions of the pulsed laser beam as shown in figure 10. When the generation source is at position A, there is a significant amount of diffraction around or transmission under the defect. The general shape of the waveform at position A in figure 12a, is similar to that at position D, but has slightly lower amplitude. Of course, one needs to perform more sophisticated signal processing to determine which modes are present in this waveform and their relative amplitude, but even the simple magnitude FFT of figure 12b reveals that there is

some significant difference between the waveforms measured for positions A and D. When the pulsed laser beam generation source is located close to the defect, at position B, both the A-scan and the FFT of figures 12 a&b show that the slot has affected the detected waveform significantly, although the higher frequency mode at approximately 1.5 MHz appears enhanced when compared to the FFTs taken at either position A or D in figure 12b. This serves as a good illustration as why one cannot generalise which frequencies or modes of Lamb waves will be effectively "blocked" by the presence of a surface breaking crack: this will depend on several factors including properties of the generation source, the crack and the sample's morphology and elastic properties. At position C, where the laser beam is incident on the slot, some amplitude enhancement is visible in the A-scan in figure 12a, and the lower plot of 12b clearly shows, relative enhancement of the higher frequencies in the FFT of the A-scan from position C.

3.2.1 Experimental results on defective stainless steel plates

A simulated stress corrosion crack was grown in a 10mm thick austenitic 316 stainless steel plate using controlled thermal fatigue loading to produce a crack 16.6mm long and 3+/-0.6mm deep, with an average crack opening of 23.8μm, as shown in figure 13. The crack depth is known through destructive validation, and also verified by ACPD measurements.

The EMAT coil is aligned parallel to the length of the defect for this particular test and the EMAT-crack separation is fixed at 7.7 cm. The pulsed laser beam is scanned across the defect with a separation range of 9.5-4.2cm from the EMAT, along a line that passes through the centre of the crack and the EMAT. A reduction in signal amplitude is observed when the defect lies between the laser beam impact point and the EMAT. This is shown in figures 14a&b, where the time domain and frequency domain data are both plotted as B-scans. The B-scans of figure 14 are more complex than those in figure 11, due to the increased number of modes present associated with the increased sample thickness. However, similar features can be observed to those reported in figure 11, including a high frequency enhancement in the frequency domain B-scan, and the minimum signal being detected when the laser beam impact point is close to the defect.
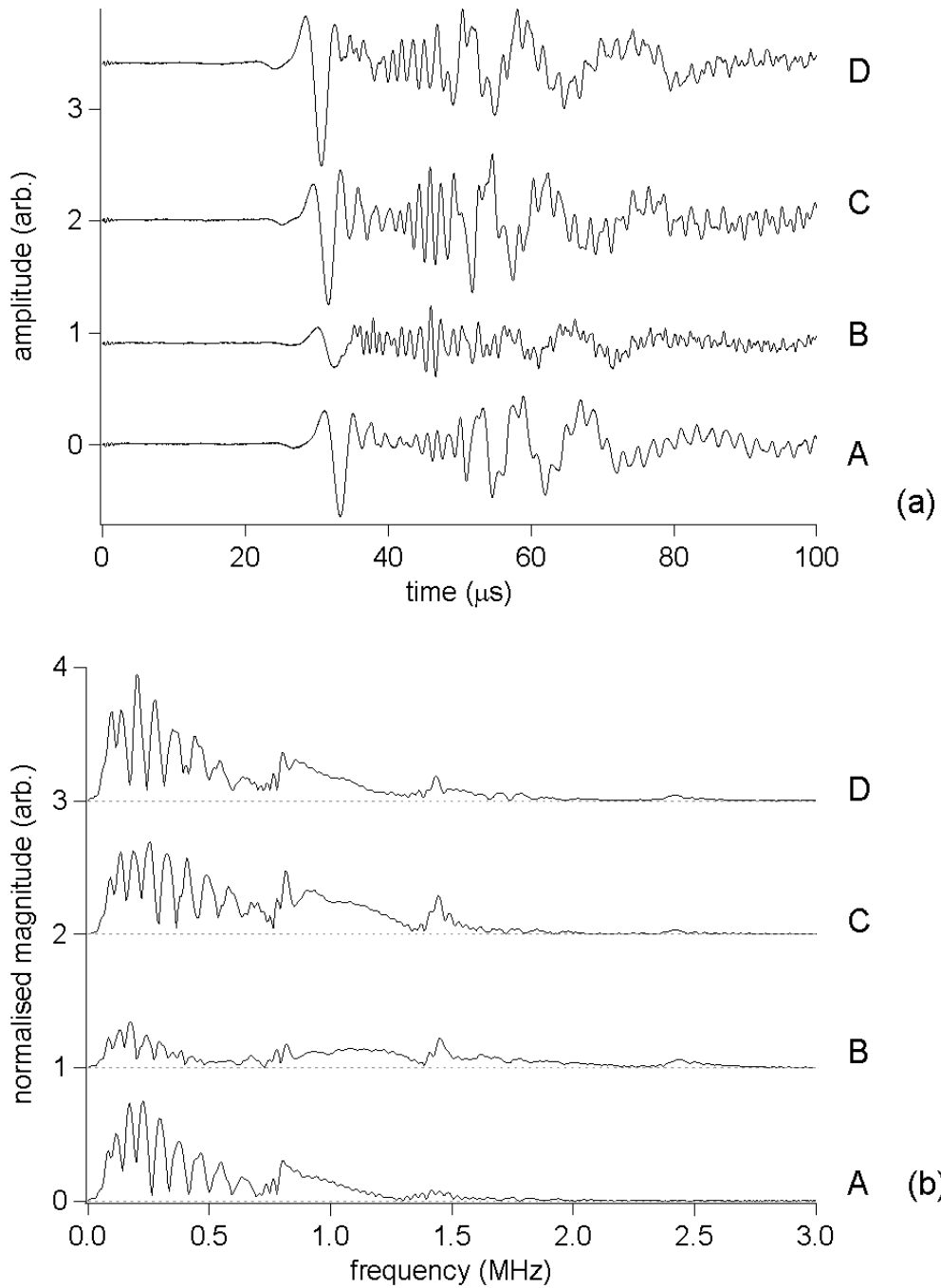
Figure 12

The upper plot (a) shows A-scan waveforms measured on the aluminium sheet taken at the positions shown on figure 10. Note that when the generation source is at position A, there is clearly a significant amount of diffraction around or transmission under the defect. Some amplitude enhancement is visible with the generation source at position C. The lower plot (b) shows the FFT of the A-scans of the upper plot (a). The enhancement of the frequency content is evident only in the lower plot (b) of the FFT.
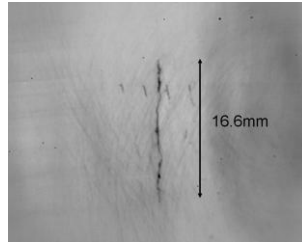
Figure 13

Photograph of simulated stress corrosion crack in austenitic steel plate. Defect is 16.6mm long and 3 +/-0.6mm deep with an average gape of 24 µm. The other marks visible around the large central cracks are polishing scratches.
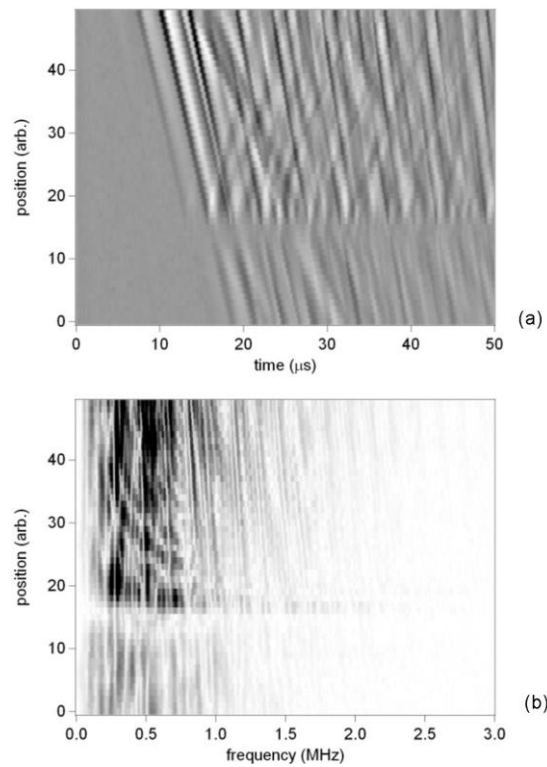

Figure 14

The B-scan of the time domain (A-scan) waveforms for the stainless steel plate containing the crack is shown in plot (a), and the B-scan of the frequency domain (magnitude FFT) waveforms of these A-scan waveforms is shown in plot (b). Note that there is a sharp drop in both the A-scan amplitude and the FFT magnitude between positions14- 16, which corresponds to the pulsed laser beam being close to the crack, with the crack positioned between the laser beam and the detection transducer. There is again a clear enhancement of the higher frequency components of the Lamb waves when the laser beam is incident on the crack at positions 17 and 18.

4. Discussion and Conclusion

The previously reported frequency enhancement of laser generated Rayleigh waves when the laser beam illuminates a crack [29-31] also occurs for thin samples where Lamb waves are generated. Laser generated Lamb waves can clearly propagate around cracks by diffraction and also under cracks. The extent to which this occurs is frequency and plate thickness dependent. The frequency of the Lamb wave clearly affects the extent to which the Lamb wave will diffract around a defect, and one must also consider the fact that the generation source is broadband. The frequency-plate thickness product also determines which modes can exist at that value of frequency-thickness and it determines also the specific properties of one particular mode and how the displacement associated with that mode is distributed through the plate thickness. One might reasonably expect the extent to which a crack impedes the propagation of Lamb wave energy to be maximum when the generation spot it closest to the defect, when the defect lies between generation and detection point, but the exact nature of this mechanism is complex and depends on many variables including the properties of the generation source, the crack and the sample's morphology and elastic properties. An attempt to provide a detailed quantitative analysis of the effects observed when the pulsed laser beam impacts directly on a crack is beyond the scope of this paper. This will be an area of future work, that will be required if quantitative measurements of crack depth is to be obtained. The main purpose of this paper is to report the potential of this non-contact ultrasonic technique using simple signal analysis, the general effects that have been observed in the time and frequency domain waveforms, and to explain the appearance of the results that have been presented using an EMAT detector. Future work will also involve analysing the directivity of the Lamb waves when the pulsed laser beam is incident upon cracks of different depths and the effect of crack depth on the frequency enhancement. The angle of the planar surface of the crack relative to the surface of the sample will also have some effect on the detected signal and this will also be investigated.

6. References

[1] White RM. Generation of elastic waves by transient surface heating. J. Appl. Phys. 34, 1963, pp3559-3564

[2] Birnbaum G, White GS. Laser techniques in NDE. In: R.S. Sharpe (Ed.), Research Techniques in Nondestructive Testing, Academic Press, New York, 1984

[3] Hutchins DA, Dewhurst RJ, Palmer SB. Applications of laser-generated ultrasound in metals. IEEE Trans Son. Utrason., 29, 1982, pp176-176

[4] Scruby CB and Drain LE. In:*Laser Ultrasonics: Techniques and applications*, Adam Hilger, Bristol (1990), p76

[5] Davies SJ, Edwards C, Taylor GS, et al., J. Phys. D: Applied Physics 26, 1993, pp329-348

[6] Hong, Y, Sharples, SD, Clark, M, et al., Rapid and accurate analysis of surface and pseudo-surface waves using adaptive laser ultrasound techniques. Ultrasonics 42, 2004, pp515-8

[7] Moura A, Lomonosov AM, Hess P. Depth evaluation of surface-breaking cracks using laser-generated transmitted Rayleigh waves. J. Appl. Phys., 2008, 103, Art. No: 084911

[8] Yashiro S, Takatsubo J, Miyauchi H, et al. A novel technique for visualizing ultrasonic waves in general solid media by pulsed laser scan. NDT & E Int., 41, 2008, pp137-144

[9] Thomsen C, Surface generation and detection of phonons by picosecond light-pulses
Phys. Rev. B 34, 1986, pp4129-4138

[10] Achenbach JD. Wave propagation in elastic solids. New York:North Holland; 1984

[11] Rose JL, Ultrasonic waves in solid media, Cambridge University Press; 2008

[12] Thompson RB, New emat configuration for generating SH-waves in ferromagnetic materials, IEEE Trans. Son. Ultrason. 26, 1979, pp149-149

[13] Hirao M and Ogi H. EMATs for science and industry : non-contacting ultrasonic measurements, Kluwer Academic Publishers, 2003

[14] Kawashima K, Quantitative Calculation and Measurement of Longitudinal and Transverse Ultrasonic Wave Pulses in Solid, 31, Issue 2, 1984, pp83-93

[15] Dixon S, Edwards C and Palmer SB, High accuracy non-contact ultrasonic thickness gauging of aluminium sheet using electromagnetic acoustic transducers, Ultrasonics 39, 2001, pp445-453

[16] Dewhurst RJ, Edwards C, McKie ADW, Palmer SB. Estimation of the thickness of thin metal sheet using laser generated ultrasound, Appl. Phys Lett. 51, 1987, pp1066-8

[17] Bushell AC, Edwards C and Palmer SB, Laser-generated surface-waves on plates of varying thickness, Brit. J. Non-destr. Test, 33, 1991, pp177-182

[18] Hutchins DA, Jansen DP and Edwards C, Lamb-wave tomography using noncontact transduction, Ultrasonics 31, 1993, pp97-103

[19]Guo ZQ, Achenbach JD and Krishnaswamy S, EMAT generation and laser detection of single lamb wave modes, Ultrasonics 35, 1997, pp423-429

[20] Dixon S, Edwards C and Palmer SB, A laser-EMAT system for ultrasonic weld inspection, Ultrasonics 37, 1999, pp273-281

[21] Murfin AS, Soden RAJ, Hatrick D et al, Laser-ultrasound detection systems: a comparative study with Rayleigh waves, Meas. Sci. Tech. 11, 2000, pp1208-1219

[22]Stepanishen P, Forbes M, Letcher S. The relationship between the impulse-response and angular spectrum methods to evaluate acoustic transient fields, J. Acous. Soc. Am. 90, 1991, pp2794-8,

[23] Dover WD, Bond LJ. Crack characterization in welded nodes as found in offshore structures using acpd and ultrasonic techniques, Mat. Eval. 43, 1985, pp1330-1330

[24] Jian X, Dixon S and Palmer SB, In-plane and out-of-plane particle velocity measurement using electromagnetic acoustical transducers, 2005 IEEE Ultrason. Symp., pp1276-1279

[25] Wilcox PD, A rapid signal processing technique to remove the effect of dispersion from guided wave signals, IEEE Trans. UFFC 50, 2003, pp419-427

[26] Alleyne D and Cawley P, A 2-dimensional Fourier-transform method for the measurement of propagating multimode signals, J. Acous. Soc. Am. 89, 1991, pp1159-1168

[27] Staszewski WJ, Pierce SG, Worden K et al., Wavelet signal processing for enhanced Lamb-wave defect detection in composite plates using optical fiber detection, Opt. Eng. 36,1997, pp1877-1888

[28] Costley RD and Berthelot YH, Dispersion curve analysis of laser-generated lamb waves, Ultrasonics 32, 1994, pp249-253

[29] Kromine AK, Fomitchov PA, Krishnaswamy S et al. Laser ultrasonic detection of surface breaking discontinuities: Scanning laser source technique, Mat. Eval. 58, 2000, pp173-177

[30] Yan Z and Nagy PB, Enhanced laser generation of surface acoustic waves by discontinuities. In: D.O.Thompson and D.E.Chimenti, Editors, Review of progress in quantitative nondestructive evaluation, American Institute of Physics, 2001, pp204-211

[31] Dixon S, Cann B, Carroll DL, et al. Non-linear enhancement of laser generated ultrasonic Rayleigh waves by cracks. Nondestr. Test Eval., 2008, 23, pp25-34